Catalysis Today 175 (2011) 117–123

Contents lists available at ScienceDirect

Catalysis Today

journal homepage: www.elsevier.com/locate/cattod

Different valent ions-doped cerium oxides and their catalytic performances for soot oxidation

Jian Liu [a], Zhen Zhao [a,*], Yongsheng Chen [b], Chunming Xu [a], Aijun Duan [a], Guiyuan Jiang [a]

[a] State Key Laboratory of Heavy Oil Processing, College of Science, China University of Petroleum, Beijing, 102249, China
[b] EMS Energy Institute and Department of Energy and Mineral Engineering, the Pennsylvania State University, University Park, PA 16802, USA

ARTICLE INFO

Article history:
Received 10 October 2010
Received in revised form 1 May 2011
Accepted 24 May 2011
Available online 20 July 2011

Keywords:
CeO_2
Doped ions
Catalysts
Nanometer
Soot oxidation

ABSTRACT

The nmCeO_2 and $Ce_{0.8}M_{0.2}O_2$ (M = Sm, Zr, V) nanoparticles were prepared by the method of microwave-assisted heating decomposition. Their catalytic performances for diesel soot oxidation were investigated with temperature-programmed oxidation reaction (TPO). Spectroscopic techniques (XRD, Raman, UV-Vis DRS and FT-IR) were utilized to characterize the structures of nmCeO_2 and $Ce_{0.8}M_{0.2}O_2$ catalysts. The results show that the structures of the catalysts depend on the different doped ions. $Ce_{0.8}Sm_{0.2}O_2$ and $Ce_{0.8}Zr_{0.2}O_2$ still preserved a face-centered cubic fluorite structure of CeO_2. However, $CeVO_4$ crystallite was formed as V doping ($Ce_{0.8}V_{0.2}O_2$). Nanometer CeO_2, $Ce_{0.8}Sm_{0.2}O_2$ and $Ce_{0.8}Zr_{0.2}O_2$ exhibited higher catalytic activity than conventional CeO_2 and $Ce_{0.8}V_{0.2}O_2$ for soot combustion due to the nanometer effect and the good contact between the catalyst and soot. For soot oxidation, nmCeO_2 is mainly active components. However, the doping of Sm or Zr could remarkably improve the thermal stability of nmCeO_2, and the doping of Sm or V could enhance the ability to resist SO_2 poison of catalysts.

1. Introduction

Cerium oxide containing materials have been the subject of numerous investigations in recent years because of their very broad range of applications in catalysis and in advanced ceramic materials. As a catalyst and catalyst promoter, ceria and ceria containing materials are used in many processes such as the treatment of automobile exhaust gases as a component in three-way catalysts (TWC). The success of ceria in diverse applications is mainly due to its unique combination of an elevated oxygen transport capacity coupled with the ability to shift easily between reduced and oxidized states ($Ce^{3+} \leftrightarrow Ce^{4+}$) [1]. Despite its widespread applications, the use of pure cerium dioxide is highly discouraged because it is poorly thermostable as it undergoes sintering at high temperatures, thereby losing its crucial oxygen storage and release characteristics. To improve its thermal stability and ability to store and release oxygen during operations, other transition and rare earth metal ions (Ti^{4+}, Zr^{4+}, La^{3+}, etc.), are normally introduced into the ceria cubic structure. The redox and catalytic property of CeO_2 is strongly influenced when it is combined with other transition metals or rare earth oxides.

Soot particulate is a serious component of air pollution and is harmful for both human beings and environment. The combination of traps and oxidation catalysts appears to be one of the most plausible after treatment technique. In this case, the catalytic oxidation for lowering the combustion temperature of soot has been performed and extensively investigated. Many kinds of catalysts have been studied for soot combustion applications, including single and mixed transition metal oxides [2,3], perovskite- and spinel-type oxides [4–7], low melting points compounds [8,9], and noble metal platinum catalysts [10,11]. Because CeO_2 plays an important role in gasoline engine exhaust three-way catalyst and its excellent oxygen storage-release and oxidation–reduction function, there are many researches on cerium base oxide catalyst for carbon particle of diesel engine exhaust. Zhu et al. [12] prepared a series of Ce–Zr oxide support loading KNO_3 catalyst. When the catalyst and soot particulates contacted in loose style, soot combustion peak temperature was below 400 °C. Weng et al. [13] and Fang et al. [14] prepared Ce–Zr nanopowder composite oxide catalyst, which had high catalytic activity on soot combustion. Aneggi et al. [15] and Atribak et al. [16] studied the structured morphology of CeO_2, TiO_2 and ZrO_2, and investigated these three oxides catalytic properties for soot particulate combustion. They found TiO_2 exists in the form of rutile and anatase crystal, and ZrO_2 is in the form of monocline or square crystalloid. The difference between the two crystalline structure square crystalloids, is no effect on soot combustion. CeO_2 exists mainly in the form of cubic fluorite structure. Among these three oxides, CeO_2 has the best oxidation activity for soot combustion. This is because, compared to the other two oxides, CeO_2 has the function to convert NO to NO_2. In addition, CeO_2 can convert CO to CO_2, which has high selectivity of CO_2. Krishna et al. [17] stud-

* Corresponding author. Tel.: +86 10 89731586; fax: +86 10 69724721.
E-mail addresses: zhenzhao@cup.edu.cn (Z. Zhao), yongsheng@psu.edu (Y. Chen).

0920-5861/$ – see front matter © 2011 Elsevier B.V. All rights reserved.
doi:10.1016/j.cattod.2011.05.023

ied the soot oxide catalytic properties under a loose contact with the catalyst of rare-earth modified CeO_2, with feed gas containing NO and O_2. The results showed that the samples combustion activity modified by Pr and La is higher than the samples non-modified. Though CeO_2 and CeO_2-related catalysts have been studied for soot oxidation in reported literature and our previous work [3], the doping with different valence ions into CeO_2 framework was not well investigated.

The catalytic oxidation of soot supposedly takes place at the three-phase boundary among a solid catalyst, a solid reactant (soot) and gaseous reactants (O_2, NO). One of the most crucial issues affecting the performance of catalysts for soot combustion is the contact efficiency between catalyst and soot [7–10]. Therefore, as described by Neeft et al., the "mobility" of catalyst plays a key role in the catalytic combustion of soot under the loose contact condition between catalyst and soot [18]. The surface particle sizes of nanometric catalyst are so small that their surface atoms have extra and high surface energy. It causes that these surface atoms are good at mobility. Thus, the contact is very good between catalyst and soot even if under the loose contact condition. Moreover, the number of active sites on the surface of the nanometer catalyst, especially the number of unsaturatedly coordinated sites is greater than non-nanometric ones. Thus, their ability to adsorb and activate oxygen is stronger than the catalyst with big particle sizes.

In this work, nanometric CeO_2 doped with different valent ions catalysts have been prepared and tested for soot oxidation, and the effects of the doped ions on the structure and on performances of catalysts for soot oxidation were investigated, and the role of nanometer effects for soot combustion was discussed.

2. Experimental

2.1. Catalyst preparation

The n$mCeO_2$ and $Ce_{0.8}M_{0.2}O_2$ (M = Sm, Zr, V) nanoparticles were prepared by the means of microwave-assisted heating decomposition. The metal nitrates or NH_4VO_3 were used as starting materials. The chemicals used for catalyst preparation were of analytical grade. Typical, an aqueous solution (pH = 4.4) containing 0.000008 mol/m^3 $Ce(NO_3)_3$, 0.000002 mol/m^3 $Sm(NO_3)_3$ (or $Zr(NO_3)_3/NH_4VO_3$), 1 wt% polyethylene glycol and 1 wt% sodium acetate (CH_3COONa) was put into a quartz vessel in the microwave reaction system under atmosphere pressure. The microwave system (Millestone Ethos 1600) operated at 2450 MHz frequency. The solution was treated under microwaves for 30 min at 90 °C. The resulting precipitation, cooled to room temperature, was centrifuged and washed with distilled water for five times and finally dried at 110 °C for 6 h. Finally, the precursor was calcined at 600 °C for 4 h in a static air. The samples will be generically named as $Ce_{0.8}M_{0.2}O_2$. The conventional CeO_2 was purchased from Ruier Rare Earth Reagent Company in China.

2.2. Catalyst characterization

The crystal structures of the fresh samples were determined by a powder X-ray diffractometer (Shimadzu XRD 6000), using Cu Kα radiation combined with Nickel filter operating at 40 kV and 10 mA. The diffractometer data were recorded for 2θ values between 10 and 80° with a 0.02° step size. The patterns were compared with JCPDS reference data for phase identification. The crystal sizes were determined with XRD data of the (1 1 1) crystalline face diffraction according to the Scherrer equation. The surface morphologies of nanometer $Ce_{0.8}M_{0.2}O_2$ samples were observed by SEM (S-4800, Japan).

Raman spectra were performed on LabRAM HR spectrometer manufactured by Horiba Jobin Yvon Company, France. The laser excitation wavelength was 514 nm. The UV-Vis NIR DRS experiments were performed on Hitachi U-4100 UV-Vis NIR spectrophotometer with the integration sphere diffuse reflectance attachment. The powder samples were loaded in a transparent quartz cell and were measured in the region of 200–800 nm at room temperature. Pure $BaSO_4$ was used as reference sample.

FT-IR absorbance spectra were obtained in the wave number ranging from 4000 to 400 cm^{-1} via a FTS-3000 spectrophotometer manufactured by American Digilab Company. 150 mg pellet was produced by pressing a mixture of each treated catalyst and KBr (1:100 weight ratio). For in situ diffuse reflection infrared Fourier transformed (DRIFT) experiments, it did not need to use KBr as diluent. The spectra were recorded in the range of 400–4000 cm^{-1} after 256 scans at a resolution of 4 cm^{-1}. The powder sample was placed in a sample holder assembly in a Harrick Praying Mantis DRIFT cell. The gases were supplied by individual mass flow controllers with a total flow rate of 50 ml/min. Before reactant gases entering, the sample was pretreated with 5% O_2 in helium at 300 °C for 30 min. The sample was then cooled to reaction temperature and equilibrated in a helium atmosphere. After the sample had cooled to the reaction temperature, a spectrum of the treated sample was taken as the background at that temperature. The in situ experiment was performed by the introduction of 2000 ppm NO (or 800 ppm SO_2) and 5% O_2 in helium. Meanwhile, the IR spectra were sequentially recorded at 400 °C for the different samples.

2.3. Catalytic activity measurement

The catalytic oxidation activities of the prepared samples were evaluated with TPO reactions and carried out on a fixed-bed tubular quartz system. The reaction temperature was controlled through a PID-regulation system based on the measurements of a K-type thermocouple and varied from 200 °C to 600 °C at a 2 °C/min rate during each TPO run. The soot used in this work was Printex-U which was supplied by Degussa as a model soot. Its primary particle size was 25 nm and specific surface was 100 m^2/g. Catalyst and soot were mixed at a mass ratio of 10:1 with a spatula in order to reproduce the loose contact mode, which is the most representative model of diesel particles flowing through a catalytic filter [3,18]. 100 mg of the mixture was placed in the tubular quartz reactor (d_i = 6 mm). Reactant gases containing 5% O_2 and 2000 ppm NO balanced with He were passed through a mixture of the catalyst and soot at a flow rate of 50 ml/min. The outlet gas composition from the reactor passed through a 1 cm^3 sampling loop of a six-point gas-sampling valve before it was being injected into an on-line gas chromatograph (GC). The GC with a flame ionization detector (FID) was used to determine CO and CO_2 concentrations after separating these gases over a Porapak N column and converting them to methane over a Ni catalyst at 380 °C. The catalytic activity was evaluated by the ignition temperature, "$T_{i''}$, which was defined as the temperature at which 10% of the soot was oxidized, and the peak temperature of CO_2 for soot combustion during TPO (T_m). The selectivity to CO_2 (S_{CO_2}) was defined as that the CO_2 outlet concentration (C_{CO_2}) divided by the sum of the CO_2 and CO outlet concentration, i.e.,

$$S_{CO_2} = \frac{C_{CO_2}}{C_{CO} + C_{CO_2}}$$

$S^m_{CO_2}$ was denoted to the S_{CO_2} at the T_m temperature. The thermal stability of catalysts was investigated by five-cycle TPO runs or testing the catalytic activity of the samples calcined at 800 °C for 20 h. The ability to resist SO_2 poison of catalysts was also studied by

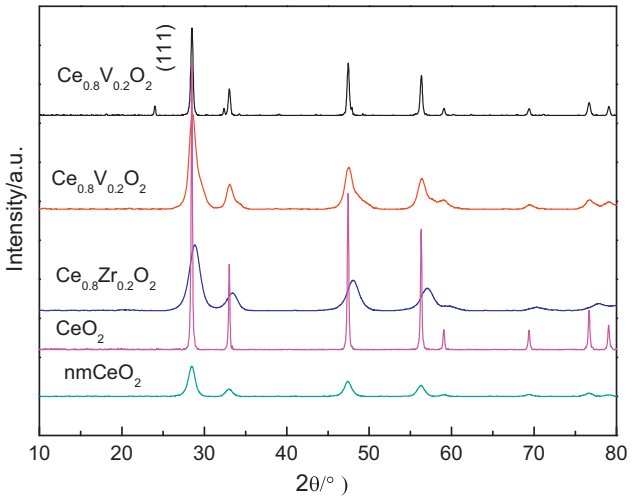

Fig. 1. X-ray diffraction patterns of CeO_2, $nmCeO_2$ and $Ce_{0.8}M_{0.2}O_2$ (M = Sm, Zr, V).

testing the catalytic activity of the samples calcined under 800 ppm SO_2 + 5% O_2 atmosphere at 700 °C for 6 h.

3. Results and discussion

3.1. Catalyst characterization

3.1.1. Results of XRD and SEM

The XRD patterns of conventional CeO_2, nanometer CeO_2 and $Ce_{0.8}M_{0.2}O_2$ (M = Sm, Zr, V) catalysts are illustrated in Fig. 1. The $Ce_{0.8}Sm_{0.2}O_2$ and $Ce_{0.8}Zr_{0.2}O_2$ samples show the diffraction peaks for (1 1 1), (2 0 0), (2 2 0), (3 1 1), (4 0 0), (3 3 1), and (4 2 0) crystal faces, corresponding to a face-centered cubic (fcc) fluorite structure for CeO_2 (JCPDS Card No. 43-1002). $Ce_{0.8}Zr_{0.2}O_2$ solid solution material was produced due to the similar ionic radii of Ce^{4+} and Zr^{4+}. Thus, zirconium ion is very easy to substitute cerium ion into the crystal lattice of $nmCeO_2$. For $Ce_{0.8}Sm_{0.2}O_2$ sample, the incorporation of samarium into the ceria lattice should result in a shift to lower angles due to the larger volume cell, but according the XRD result in Fig. 1, a shift to higher angles and a tail were found in the diffraction profile of $Ce_{0.8}Sm_{0.2}O_2$, indicating that $Ce_{0.8}Sm_{0.2}O_2$ sample did not form the solid solution. For $Ce_{0.8}V_{0.2}O_2$ sample, several diffraction peaks at ~24°, 32°, and 48° appeared in the XRD patterns due to the formation of crystal phase of $CeVO_4$ (JCPDS Card No. 84-1457) [1,19]. No V_2O_5 crystal phase was detected by XRD. It indicated that vanadium oxide selectively interacted with the ceria portion of these mixed oxides and formed the stable compound. The crystalline size of nanometer CeO_2 calculated using Scherrer formula was around 7 nm, and the crystalline sizes of $Ce_{0.8}Sm_{0.2}O_2$ and $Ce_{0.8}Zr_{0.2}O_2$ catalysts are in the range of 6–8 nm as shown in Table 1. For $Ce_{0.8}V_{0.2}O_2$, the crystalline sizes increase to 26 nm, which may be due to the formation of $CeVO_4$ crystal phase. Fig. 2 shows SEM photographs of $nmCeO_2$ and $Ce_{0.8}M_{0.2}O_2$ samples. It can be seen that the particle sizes of $nmCeO_2$, $Ce_{0.8}Sm_{0.2}O_2$ and $Ce_{0.8}Zr_{0.2}O_2$ samples were between 40 and 60 nm, and the catalyst particles were similar to spherical shape. Therefore, these results reveal that these catalysts which were prepared by the microwave-assisted heating decomposition method possessed nanometer particle sizes. However, the SEM photograph of $Ce_{0.8}V_{0.2}O_2$ exhibits that the catalyst particles had an average particle size at around 500 nm. The larger particle sizes observed from the SEM images than the crystallite sizes mea-

Table 1
The average crystal parameters of CeO_2, $nmCeO_2$ and $Ce_{0.8}M_{0.2}O_2$ (M = Sm, Zr, V).

Catalysts	Crystal face	λ/nm	2θ/°C	β/°C	D/nm
$nmCeO_2$	1 1 1	0.1542	28.4541	1.1580	7.00
CeO_2	1 1 1	0.1542	28.5072	0.1981	40.95
$Ce_{0.8}Sm_{0.2}O_2$	1 1 1	0.1542	28.6597	1.0268	7.90
$Ce_{0.8}Zr_{0.2}O_2$	1 1 1	0.1542	28.6895	1.1812	6.87
$Ce_{0.8}V_{0.2}O_2$	1 1 1	0.1542	28.4975	0.3082	26.32

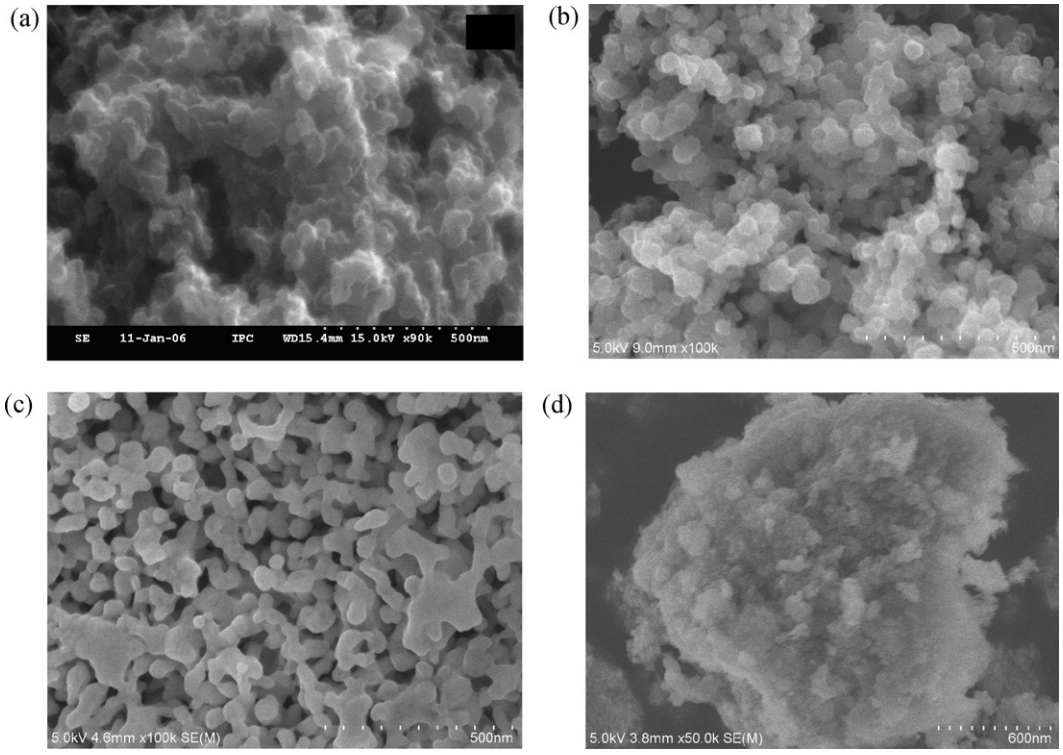

Fig. 2. SEM photographs of $nmCeO_2$ and $Ce_{0.8}M_{0.2}O_2$ (M = Sm, Zr, V) (a) $nmCeO_2$, (b) nm $Ce_{0.8}Sm_{0.2}O_2$, (c) nm $Ce_{0.8}Zr_{0.2}O_2$ and (d) nm $Ce_{0.8}V_{0.2}O_2$.

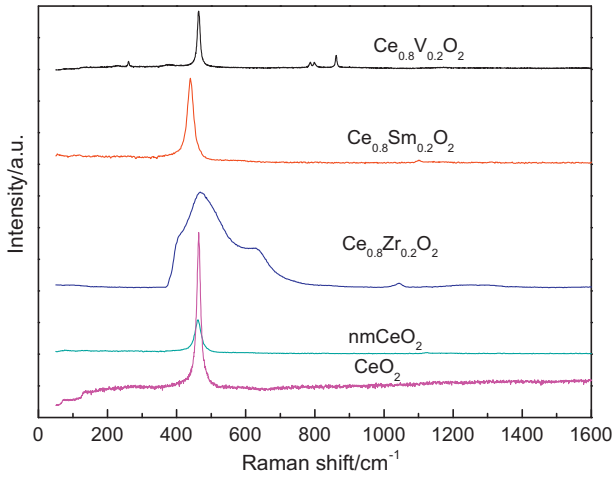

Fig. 3. Raman spectra of CeO_2, $nmCeO_2$ and $Ce_{0.8}M_{0.2}O_2$ (M = Sm, Zr, V).

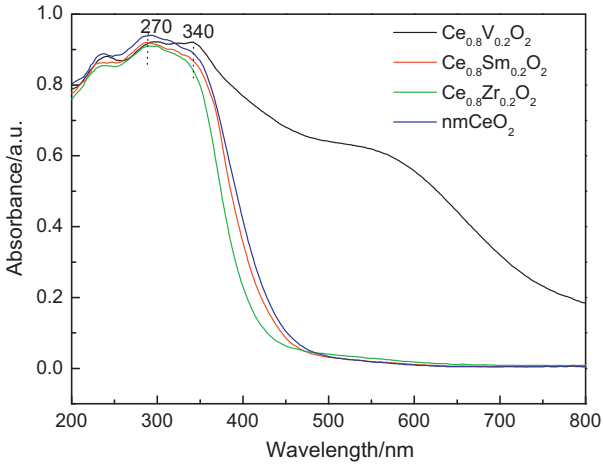

Fig. 4. UV-Vis NIR spectra of $nmCeO_2$ and $Ce_{0.8}M_{0.2}O_2$ (M = Sm, Zr, V).

sured by XRD illustrates that powder particles were agglomerated to some extent.

3.1.2. Raman characterization

Raman characterization technique has been successfully used to determine the surface structures of oxide because Raman spectroscopy directly probes structures and bonds by their spectra. As shown in Fig. 3, the Raman spectra of conventional CeO_2, nanometer CeO_2 and $Ce_{0.8}M_{0.2}O_2$ exhibit a prominent peak at about 464 cm^{-1}. This band is corresponding with the triply degenerate F_{2g} mode and can be viewed as a symmetric stretching mode of the oxygen atoms around cerium ions [19–21]. The spectrum of $Ce_{0.8}Zr_{0.2}O_2$ sample is again dominated by a strong band at 464 cm^{-1} and a broad shoulder peak at ~600 cm^{-1}. It is apparent from Raman results that ceria–zirconia is mostly in the cubic form and did not show signs of tetragonal modification. The shift in the Raman frequency to higher wavenumbers could be due to incorporation of zirconia into the ceria lattice. Some new bands are also observed at ~796 and 857 cm^{-1} for $Ce_{0.8}V_{0.2}O_2$ samples. These bands are due to the formation of $CeVO_4$. No crystalline V_2O_5 features (Raman bands at ~995, 702, 527, 404, 284, and 146 cm^{-1}) were found, which is in agreement with the XRD observations. It is proposed that the VO_4^{3-} surface species existing on the $Ce_{0.8}V_{0.2}O_2$ will be integrated together under the influence of high-temperature calcinations and interact with the ceria to form the stable $CeVO_4$ compound. Therefore, it decreases the amount of dispersed vanadium oxide on the surface of the support. According to literature reports [20,21], the tetrahedral VO_4^{3-}, as present in aqueous solution, has the most prominent Raman band at 827 cm^{-1}, and for solids, with isolated VO_4^{3-} units, this band lies in the range 830–855 cm^{-1}. It is associated with the stretching mode of the vanadium tetrahedron. In $CeVO_4$, vanadium ions are placed at the centers of oxygen tetrahedral with a vanadium–oxygen distance similar to that of an isolated VO_4^{3-}. Therefore, the band at 857 cm^{-1} of $CeVO_4$ can be assigned to such a mode. The Raman results support the formation of $CeVO_4$ in the catalyst even if the initial atomic ratio of Ce to V is 4:1.

3.1.3. UV-Vis DRS characterization

The UV-Vis DRS spectroscopy can be applied to investigate the structures of $Ce_{0.8}M_{0.2}O_2$ catalysts due to the ligand-to-metal charge transfer (LMCT) transitions of metal ions in the 200–500 nm region and d–d transition bands in the 600–800 nm region originating from d–d electron transferring. The characterization gives rise to very qualitative information. The local structures of doping ions in these materials are often associated with the band positions of the LMCT transitions [22,23]. The DRS spectra of $Ce_{0.8}M_{0.2}O_2$ catalysts are presented in Fig. 4. For $nmCeO_2$ and $Ce_{0.8}M_{0.2}O_2$ samples, there was a broad absorption band around 200–400 nm which was assigned to the LMCT transitions. Both of them exhibit strong absorption bands centered at ca. 270 and 340 nm in the UV range, which originate from the charge-transfer between the O 2p and Ce 4f states in O^{2-} and Ce^{4+} [22]. This spectral profile indicates that the charge-transfer transition of Ce^{4+} overlaps with the $4f^1 \rightarrow 5d^1$ transition of Ce^{3+}. For $nmCeO_2$, $Ce_{0.8}Sm_{0.2}O_2$ and $Ce_{0.8}Zr_{0.2}O_2$ samples, no absorption was detected above 500 nm in wavelength, indicating that no d–d electron transferring took place in these catalysts. A clear blue shifting of the absorption threshold edge can be observed for $Ce_{0.8}Sm_{0.2}O_2$ and $Ce_{0.8}Zr_{0.2}O_2$, contrasting with $nmCeO_2$ samples. The LMCT transitions of $Ce_{0.8}V_{0.2}O_2$ are broader than those of the other catalysts. Moreover, its d–d transition band in the 600–800 nm region originating from d–d electron transferring is also observed.

3.1.4. FT-IR characterization

FT-IR spectroscopy gave some information about the structures of the catalysts. Fig. 5 shows that $nmCeO_2$ and $Ce_{0.8}M_{0.2}O_2$ display a big absorption band below 600 cm^{-1}, which is assigned to the

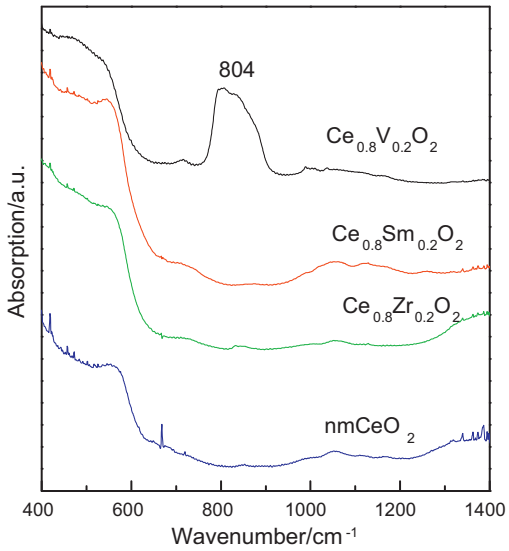

Fig. 5. IR absorbance spectra of $nmCeO_2$ and $Ce_{0.8}M_{0.2}O_2$ (M = Sm, Zr, V).

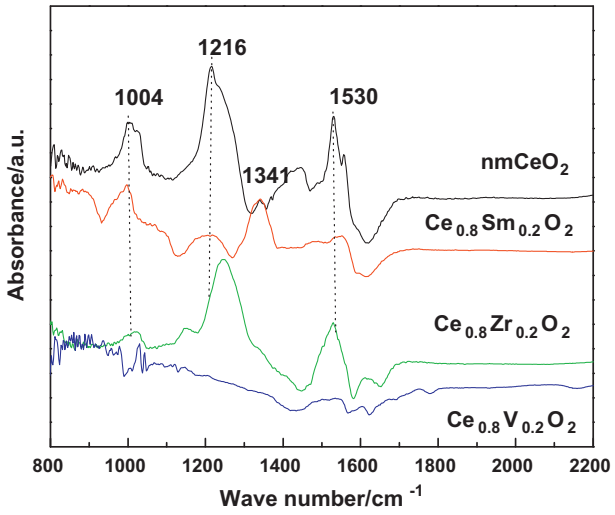

Fig. 6. In situ DRIFT spectra of $nmCeO_2$ and $Ce_{0.8}M_{0.2}O_2$ at 400 °C under the NO + O_2 atmosphere (M = Sm, Zr, V).

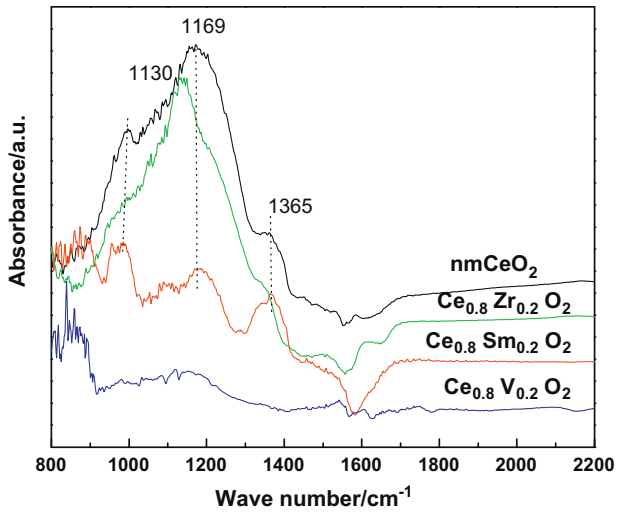

Fig. 7. In situ DRIFT spectra of $nmCeO_2$ and $Ce_{0.8}M_{0.2}O_2$ at 400 °C under the SO_2 + O_2 atmosphere (M = Sm, Zr, V).

Ce–O stretching vibration of CeO_2. As shown in Fig. 5, $Ce_{0.8}V_{0.2}O_2$ exhibits a big absorption band centered at 800 cm^{-1} and a small peak at 1024 cm^{-1}. The former is due to the $CeVO_4$ formation on the surface, and the latter may be due to the vibration of V=O bond of isolated VO_4^{2-} [24].

The in situ DRIFT spectra during exposure of $nmCeO_2$ and $Ce_{0.8}M_{0.2}O_2$ catalysts to 2000 ppm NO and 5% O_2 at 400 °C are shown in Fig. 6. The adsorbed species are attributed predominantly to various nitrites and nitrates, as well as other nitrogen-containing species. A strong absorption band at ~1216 cm^{-1} is assigned to the bridging bidentate nitrite, and two shoulder peaks at about 1530 cm^{-1} and 1550 cm^{-1} are due to $\nu_{N=O}$ stretching vibration of chelating bidentate nitrates. The peak located at ~1004 cm^{-1} is attributed to the symmetric stretching vibration of bidentate nitrates, and a weak peak located at about 1341 cm^{-1} is ascribed to the symmetric stretching vibration of monodentate nitrates (ν_{symNO_2}) [25–30]. As shown in Fig. 6, there are very small IR peaks for NO_x adsorption over $Ce_{0.8}V_{0.2}O_2$ sample, and the introduction of Sm or Zr into the lattice of $nmCeO_2$ also weakens the NO_x adsorption on the catalysts.

The in situ DRIFT spectra during exposure of $nmCeO_2$ and $Ce_{0.8}M_{0.2}O_2$ catalysts to 800 ppm SO_2 and 5% O_2 at 400 °C are shown in Fig. 7. Free SO_4^{2-} ion, which has high symmetry of Td group, is tetrahedral structure. There are four vibrancies to IR spectra, and only the symmetry stretching vibration (v_3) and outside bending vibration (v_4) are active. Their vibration frequencies locate at 1105 and 611 cm^{-1}, respectively, according to the theory calculation [31]. Therefore, the strong absorption peaks at 1130 and 1169 cm^{-1} are ascribed to the formation of sulfate [31,32]. A weak shoulder peak at 1365 cm^{-1} is due to sulfite production on the catalysts [33]. The higher peak intensity over $nmCeO_2$ and $Ce_{0.8}Zr_{0.2}O_2$ catalysts indicates the poorer capacity to resist SO_2 poison than that of $Ce_{0.8}Sm_{0.2}O_2$ and $Ce_{0.8}V_{0.2}O_2$ catalysts.

Fig. 8 shows the IR absorbance spectra of $nmCeO_2$ and $Ce_{0.8}M_{0.2}O_2$ catalysts after calcination under the SO_2 + O_2 atmosphere. The sharp absorbance peak at 1383 cm^{-1}, which can be assigned to sulfite, was observed on the $nmCeO_2$ catalysts [33]. But this peak was not observed on IR spectra of the other catalysts. It further indicates that $Ce_{0.8}M_{0.2}O_2$ catalysts have the stronger capacity to resist SO_2 poison than that of $nmCeO_2$ catalyst.

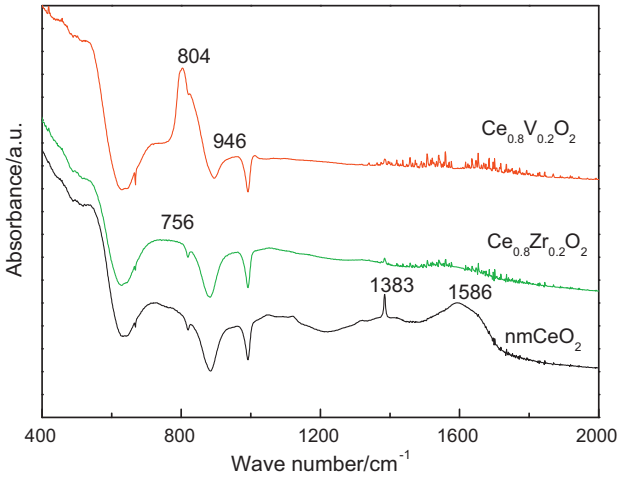

Fig. 8. IR absorbance spectra of $nmCeO_2$ and $Ce_{0.8}M_{0.2}O_2$ catalysts after calcination under the SO_2 + O_2 atmosphere (M = Zr, V).

3.2. Catalytic activity results

The oxidation activity of catalysts was examined from the standpoint of their ability to lower the combustion temperature of soot. The reproducibility of the reaction process is very important. For each TPO result, three parallel measurements were carried out and no obvious activity change was observed. In order to accurately detect the true reaction temperatures, the catalyst–soot fixed bed was sandwiched between two quartz–wool layers. And the tip of a K-type thermocouple was located well inside the catalyst bed itself. Table 2 lists the results of soot combustion in the absence

Table 2
The catalytic performances and surface areas of CeO_2, $nmCeO_2$ and $Ce_{0.8}M_{0.2}O_2$ (M = Sm, Zr, V) for soot combustion.

Catalysts	S_{BET}/g/m^2	$S^m_{CO_2}$/%	T_i/°C	T_m/°C
Soot (without catalyst)	100	44	482	594
$nmCeO_2$	48.8	90.4	379	465
CeO_2	9.4	89.1	412	487
$Ce_{0.8}Sm_{0.2}O_2$	47.2	90.5	381	466
$Ce_{0.8}Zr_{0.2}O_2$	47.8	90.2	385	469
$Ce_{0.8}V_{0.2}O_2$	15.4	88.4	399	494

Table 3
The catalytic performances for soot combustion over $nmCeO_2$ and $Ce_{0.8}M_{0.2}O_2$ (M = Sm, Zr, V) catalysts after calcination at 800 °C for 20 h under air atmosphere or at 700 °C under 800 ppm SO_2 + 5% O_2 atmosphere for 6 h and five-cycle reactions.

Catalysts	Five recycle reactions		Calcined at 800 °C under air atmosphere for 20 h		Calcined at 700 °C under 800 ppm SO_2 + 5% O_2 atmosphere for 6 h	
	$S^m_{CO_2}$/%	T_m/°C	$S^m_{CO_2}$/%	T_m/°C	$S^m_{CO_2}$/%	T_m/°C
$nmCeO_2$	89.6	483	88.6	486	88.9	499
$Ce_{0.8}Sm_{0.2}O_2$	89.9	472	89.2	481	88.4	483
$Ce_{0.8}Zr_{0.2}O_2$	90.1	472	90.1	480	88.7	494
$Ce_{0.8}V_{0.2}O_2$	88.3	498	87.2	508	87.8	509

and presence of $nmCeO_2$ and $Ce_{0.8}M_{0.2}O_2$ catalysts. It can be seen that the combustion temperature of soot in the absence of catalysts was very high (T_m = 594 °C). In the presence of $nmCeO_2$ and $Ce_{0.8}M_{0.2}O_2$ catalysts, a remarkable decrease of the temperature values was observed (T_m decreased by exceeding 120 °C). Thus, the soot combustion is favored by the presence of $nmCeO_2$ and $Ce_{0.8}M_{0.2}O_2$ catalysts. However, the catalytic activity lowered with the increase of the valence of doping ions. The decrease in soot combustion temperature was only 100 °C in the presence of $Ce_{0.8}V_{0.2}O_2$. It is due to the low catalytic activity of $CeVO_4$ and the large particle size of $Ce_{0.8}V_{0.2}O_2$ catalyst. The higher is the quantity of vanadium doped, the lower is the number of active vacant sites of nanometer ceria, and the lower are the activities of catalysts. Therefore, the doping of different valent ions in ceria plays an important role in the catalytic performances of the doped $nmCeO_2$ system catalysts for soot oxidation.

Thermal stability tests were investigated for $nmCeO_2$ and $Ce_{0.8}M_{0.2}O_2$ catalysts. Firstly, the catalytic combustion reaction of soot was carried out by five-cycle. TPO runs on $nmCeO_2$ and $Ce_{0.8}M_{0.2}O_2$ (M = Sm, Zr, V) catalysts. Secondly, the prepared samples were calcined again under the static air at 800 °C for 20 h and then the TPO tests were conducted. Table 3 shows that the change of $S^m_{CO_2}$ was unapparent, but T_i and T_m were remarkably increased after the thermal treatment. It was due to the agglomeration of nanoparticle catalysts. $Ce_{0.8}V_{0.2}O_2$ catalyst still holds the lower activity. Moreover, after the thermal treatment, T_m increased by 20 °C for soot combustion over nanometric CeO_2, but it increased by no more than 15 °C after Zr intruded into the lattice of $nmCeO_2$ oxides. Thus, the formation of solid solutions due to the incorporation of a small amount of Zr into $nmCeO_2$ may lead to the enhancement of the thermal stability of catalysts. Moreover, Table 3 also lists the catalytic activity results after the catalysts were calcined under 800 ppm SO_2 + 5% O_2 atmosphere at 700 °C for 6 h. T_m increased by 25 °C for soot combustion over $nmCeO_2$ and $Ce_{0.8}Zr_{0.2}O_2$ catalysts, but it increased by no more than 17 °C for that over $Ce_{0.8}Sm_{0.2}O_2$ and $Ce_{0.8}V_{0.2}O_2$ catalysts even if $Ce_{0.8}V_{0.2}O_2$ catalyst still held the lower activity. These results indicate that $Ce_{0.8}Sm_{0.2}O_2$ and $Ce_{0.8}V_{0.2}O_2$ catalysts have better ability to resist SO_2 poison than $nmCeO_2$ and $Ce_{0.8}Zr_{0.2}O_2$ catalysts.

3.3. Discussion

The redox and catalytic properties of ceria and its composite oxides are mainly dependent upon these main factors: particle size, phase modification, structural defects/distortion (lattice), and chemical nonstoichiometry [1]. In general, reducing the particle size of a catalyst results in increasing surface area and changing its morphology, thus it provides a larger number of more reactive edge sites. Especially, when the particle size is decreased below 100 nm, the materials become nanophase where the density of defect sites or the number of unsaturatedly coordinated sites largely increases, even up to half of the atoms are situated in the cores of defects in nanophase materials. Thus, it provides a larger number of active sites for gas–solid catalysts, while the diffusivity through the nanometer-sized interfacial boundaries promotes fast kinetics of the catalyst activation and reaction. On the other hand, the catalytic performance of catalyst is closely related to its surface area. For a given catalyst, the more the surface area of the catalyst is exposed to soot, the higher the catalytic activity of the catalyst will give. Since the nanoparticle catalysts have higher fraction of surface atoms than the conventional catalysts with large particle size, the catalyst is in close proximity to soot particle and more catalyst surface is exposed to reaction atmosphere. A decrease in particle size from 1 μm to 10 nm will increase the contact of soot and catalyst probability by 100 times. Thus, there are several advantages for switching from conventional to nanosized catalysts. As shown in Table 2, conventional CeO_2 catalyst holds the lower activity than nanometer CeO_2. T_m increased by 22 °C for soot combustion over conventional CeO_2 catalyst than that over nanometric CeO_2.

The proposed mechanism of microwave-assisted heating decomposition preparation of $nmCeO_2$ and $Ce_{0.8}M_{0.2}O_2$ nanoparticles may be similar to a general decomposition process [24]. Firstly, hydrated Ce(IV) ions can form complexes with H_2O molecules or OH^- ions. Polymers of this hydroxide, $Ce(H_2O)_x(OH^-)_y^{(4-y)+}$, can then serve as a precursor of the oxide. The starting precipitate from the Ce(IV) salt may be formed by nucleation of hydrated $Ce(H_2O)_x(OH^-)_y^{(4-y)+}$, which may lead to the formation of very fine precursors for the final oxide. In aqueous solution, water as a polar molecule tends to take protons away from coordinated hydroxide and the reaction equation can be expressed as follows: $Ce(H_2O)_x(OH^-)_y^{(4-y)+} + H_2O \rightarrow CeO_2{\cdot}nH_2O + H_3O^+$. In the microwave heating environment, the fast and homogeneous heating gives rise to a rapid and more simultaneous nucleation than the conventional method. Consequently uniformed small particles can be prepared. Polyethylene glycol as a dispersion stabilizer can inhibit non-homogeneous precipitation. Sodium acetate is used to adjust the pH value of the solution. The $nmCeO_2$ obtained by microwave irradiation was calcined at 600 °C in a muffle furnace. At this temperature all the polymer used as a dispersive stabilizer was removed. Thus, uniform nanometer $Ce_{0.8}M_{0.2}O_2$ powder can be synthesized by this method. The average crystalline diameter is about 7 nm according to Scherrer equation from XRD result for $nmCeO_2$ and $Ce_{0.8}M_{0.2}O_2$ (M = Sm, Zr). The SEM images show that the prepared sample has the particle sizes ranging from 40 to 50 nm.

Besides nanometer effect can improve the contact between soot and catalyst, the use of NO/O_2 as oxidizing agents can also enhance the contact through NO_2 intermediate. Due to the strong oxidizing ability of NO_2 and the good contact property of NO_2 molecule and soot particles, the soot combustion rate would be accelerated [10,11]. According to the in situ DRIFT results as shown in Fig. 6, it is found that NO is adsorbed and stored on the catalyst as nitrite/nitrate. The nitrates can decompose and release NO_2 to the gas phase. Then, NO_2 acts as the oxidizing agent for soot combustion. The direct evidence of NO_2 produced over nanometric CeO_2 has been detected by the means of mass spectroscopic measurement in our previous work [3]. The nitrate storage capacity of $nmCeO_2$ and $Ce_{0.8}Zr_{0.2}O_2$ samples is three to five times as that of $Ce_{0.8}V_{0.2}O_2$ sample oxide resulting in a major contribution

of the produced NO_2 to the soot oxidation. This also explains the higher catalytic activity of $nmCeO_2$ and $Ce_{0.8}Zr_{0.2}O_2$ than that of $Ce_{0.8}V_{0.2}O_2$ mixed oxide for the soot oxidation in this work.

Within the field of solid-state chemistry, oxygen storage and release properties of cerium oxides (CeO_2) have played important roles, especially in terms of automotive exhaust catalysts. CeO_2 and its related materials can lower the ignition temperatures of particulate matters (mainly soot) that are released from diesel vehicles. In recent years, therefore, much attention has been given on the synthesis and characterization of solid solutions based on CeO_2. In particular, studies have focused on CeO_2–ZrO_2, which possess significantly enhanced thermal stability, redox property, and catalytic activities (comparable to those of pure CeO_2). Numerous investigations have been carried out to determine the structure and morphology of the $Ce_xZr_{1-x}O_2$ solid solutions [13–17]. Other studies have aimed at investigating the effect of trivalent dopants such as yttria, lanthana, and praseodymia on the redox behavior and thermal stability of the CeO_2 materials [34,35]. In this study, thermal stability tests exhibit that the doping of Sm or Zr could remarkably improve the thermal stability of $nmCeO_2$, and the doping of Sm or V could enhance the ability to resist the SO_2 poison of catalysts. Although the fresh nanometric CeO_2 catalyst has better catalytic performances than the fresh $Ce_{0.8}Zr_{0.2}O_2$ and $Ce_{0.8}Sm_{0.2}O_2$ catalysts, the catalytic performances of the latter ones are reversely better than the former one after all the samples calcination again under the static air gas at 800 °C for 20 h. Similarly, as shown in Fig. 7, in situ DRIFT results exhibit that more sulfate were produced over $nmCeO_2$ and $Ce_{0.8}Zr_{0.2}O_2$ catalysts poisoned with SO_2. Thus, the ability to resist SO_2 poison of $Ce_{0.8}Sm_{0.2}O_2$ and $Ce_{0.8}V_{0.2}O_2$ catalysts were better than that of $nmCeO_2$ and $Ce_{0.8}Zr_{0.2}O_2$ catalysts. These properties could be more helpful to understand how to apply ceria containing materials under the complex reaction condition.

4. Conclusions

(1) The $nmCeO_2$ and $Ce_{0.8}M_{0.2}O_2$ (M = Sm, Zr) nanoparticles were prepared by the method of microwave-assisted heating decomposition. Their structures depend on the doping ions, and the doping of vanadium ion results in the formation of $CeVO_4$ complex oxide.

(2) Based on the catalytic performances of $Ce_{0.8}M_{0.2}O_2$ catalysts for soot combustion, they can be classified into two groups according to the different doping ions. The first group is pure nanometric CeO_2, $Ce_{0.8}Sm_{0.2}O_2$ and $Ce_{0.8}Zr_{0.2}O_2$ catalysts which can lower the temperatures of soot combustion by more than 100 °C. It is due to the nanometer effect and the good contact between the catalyst and soot. Whereas, the second one is the group of catalysts containing vanadium for which the catalytic activity is low. Thermal stability tests exhibit that $Ce_{0.8}M_{0.2}O_2$ catalysts are superior to $nmCeO_2$. And the ability to resist SO_2 poison of $Ce_{0.8}Sm_{0.2}O_2$ and $Ce_{0.8}V_{0.2}O_2$ catalysts are better than that of $nmCeO_2$ and $Ce_{0.8}Zr_{0.2}O_2$ catalysts.

Acknowledgements

This work was supported by the National Natural Science Foundation of China (Nos. 20803093, 20833011), the 863 Program of China (No. 2009AA06Z313), and CNPC Innovation Foundation (2010D-5006-0402), the NCET-10-0811 and Doctor Select Foundation for the University of State Education Ministry (No. 200804251016).

References

[1] B.M. Reddy, A. Khan, P. Lakshmanan, M. Aouine, S. Loridant, J.C. Volta, J. Phys. Chem. B 109 (2005) 3355.
[2] Z. Zhang, Y. Zhang, Z. Wang, X. Gao, J. Catal. 271 (2010) 12.
[3] J. Liu, Z. Zhao, J. Wang, C. Xu, A. Duan, G. Jiang, O. Yang, Appl. Catal. B 84 (2008) 185.
[4] W.F. Shangguan, Y. Teraoka, S. Kagawa, Appl. Catal. B 16 (1998) 149.
[5] S.S. Hong, G.D. Lee, Stud. Surf. Sci. Catal. 159 (2006) 261.
[6] J. Liu, Z. Zhao, C. Xu, A. Duan, Appl. Catal. B 78 (2008) 61.
[7] Q. Li, M. Meng, N. Tsubaki, X. Li, Z. Li, Y. Xie, T. Hu, J. Zhang, Appl. Catal. B 91 (2009) 406.
[8] J. Liu, Z. Zhao, C. Xu, A. Duan, L. Zhu, X.Z. Wang, Appl. Catal. B 61 (2005) 39.
[9] A. Setiabudi, N.K. Allaart, M. Makkee, J.A. Moulijn, Appl. Catal. B 60 (2005) 233.
[10] J. Oi-Uchishawa, A. Obuchi, S.D. Wang, T. Nanba, A. Ohi, Appl. Catal. B 43 (2003) 117.
[11] K. Hinot, H. Burtscher, A.P. Weber, G. Kasper, Appl. Catal. B 71 (2007) 271.
[12] L. Zhu, J. Yu, X. Wang, J. Hazard. Mater. 140 (2007) 205.
[13] D. Weng, J. Li, X. Wu, Z. Si, J. Rare Earths 28 (2010) 542.
[14] P. Fang, M. Luo, J. Lu, S. Cen, X. Yan, X. Wang, Thermochim. Acta 478 (2008) 45.
[15] E. Aneggi, C. de Leitenburg, G. Dolcetti, A. Trovarelli, Catal. Today 114 (2006) 40.
[16] I. Atribak, I. Such-Basánez, A. Bueno-López, A.G. García, J. Catal. 250 (2007) 75.
[17] K. Krishna, A. Bueno-Lopez, M. Makkee, J.A. Moulijn, Appl. Catal. B 75 (2007) 201.
[18] P.A.J. Neeft, M. Makkee, J.A. Moulijn, Appl. Catal. B 8 (1996) 57.
[19] J.A. Rodriguez, J.C. Hanson, J.Y. Kim, G. Liu, A.I. Juez, M.F. Garcia, J. Phys. Chem. B 107 (2003) 3535.
[20] B.M. Reddy, A. Khan, Y. Yamada, T. Kobayashi, S. Loridant, J.C. Volta, J. Phys. Chem. B 106 (2002) 10964.
[21] B.M. Reddy, A. Khan, Y. Yamada, T. Kobayashi, S. Loridant, J.C. Volta, J. Phys. Chem. B 107 (2003) 5162.
[22] S. Tsunekawa, T. Fukuda, J. Appl. Phys. 87 (1999) 1318.
[23] L.E. Briand, O.P. Tkachenko, M. Guraya, X. Gao, I.E. Wachs, W. Grunent, J. Phys. Chem. B 108 (2004) 4823.
[24] J. Liu, Z. Zhao, C. Xu, A. Duan, G. Jiang, J. Rare Earths 28 (2010) 198.
[25] B. Olthof, A. Khodakov, A.T. Bell, E. Iglesia, J. Phys. Chem. B 104 (2000) 1516.
[26] X. Zhang, H. He, H. Gao, Y. Yu, Spectrochim. Acta Part A: Mol. Biomol. Spectrosc. 71 (2008) 1446.
[27] X. Wu, F. Lin, D. Weng, J. Li, Catal. Commun. 9 (2008) 2428.
[28] J. Liu, Z. Zhao, J. Lan, C. Xu, A. Duan, G. Jiang, X. Wang, H. Hong, J. Phys. Chem. C 113 (2009) 17114.
[29] J. Liu, Z. Zhao, C. Xu, A. Duan, G. Jiang, Ind. Eng. Chem. Res. 49 (2010) 3112.
[30] J. Yu, Z. Jiang, L. Zhu, Z. Hao, Z. Xu, J. Phys. Chem. B 110 (2006) 4291.
[31] L. Li, Z. Chen, J. Ding, T. Zhu, Y. Zhang, Chin. Spectrosc. Spectrosc. Anal. 24 (2004) 1556.
[32] S. Xie, J. Wang, H. He, J. Mol. Catal. A 266 (2007) 166.
[33] W. Clark, G.M. Sverdrup, S.J. Goquen, R.L. Graves, G.F. Keller, D.L. Mckinnon, B. Bertlesen, M.J. Quinn, SAE 2000-01-1879, 2000.
[34] J.F. Lamonier, S.P. Kulyova, E.A. Zhikinskaya, B.G. Kostyuk, V.V. Lumin, A. Aboukas, Kinet. Catal. 45 (2004) 429.
[35] J. Liu, Z. Zhao, C. Xu, A. Duan, L. Wang, S. Zhang, Catal. Commun. 8 (2007) 220.